

# Integrated Luneburg lens via ultra-strong index gradient on silicon

Lucas H. Gabrielli<sup>1</sup> and Michal Lipson<sup>1,2,\*</sup>

<sup>1</sup>Cornell Nanophotonics Group, School of Electrical and Computer Engineering,  
Cornell University, Ithaca, New York 14853, USA

<sup>2</sup>Kavli Institute at Cornell, Cornell University, Ithaca, New York 14853, USA

[\\*ml292@cornell.edu](mailto:ml292@cornell.edu)

**Abstract:** Gradient index structures are gaining increased importance with the constant development of Transformation Optics and metamaterials. Our ability to fabricate such devices, while limited, has already demonstrated the extensive capabilities of those designs, in the forms of invisibility devices, as well as illusion optics and super-lensing. In this paper we present a low loss, high index contrast lens that is integrated with conventional nanophotonic waveguides to provide improved tolerance in fiber-to-chip optical links for future communication networks. This demonstration represents a positive step in making the extraordinary capabilities of gradient index devices available for integrated optics.

© 2011 Optical Society of America

**OCIS codes:** (110.2760) Gradient-index lenses; (230.3120) Integrated optics devices.

---

## References and links

1. D. Smith, J. Mock, A. Starr, and D. Schurig, "Gradient index metamaterials," *Phys. Rev. E* **71**, 036609 (2005).
2. R. B. Greegor, C. G. Parazzoli, J. A. Nielsen, M. A. Thompson, M. H. Tanielian, and D. R. Smith, "Simulation and testing of a graded negative index of refraction lens," *Appl. Phys. Lett.* **87**, 091114 (2005).
3. T. Driscoll, D. N. Basov, A. F. Starr, P. M. Rye, S. Nemat-Nasser, D. Schurig, and D. R. Smith, "Free-space microwave focusing by a negative-index gradient lens," *Appl. Phys. Lett.* **88**, 081101 (2006).
4. L. H. Gabrielli, J. Cardenas, C. B. Poitras, and M. Lipson, "Silicon nanostructure cloak operating at optical frequencies," *Nat. Photonics* **3**, 461–463 (2009).
5. J. Valentine, J. Li, T. Zentgraf, G. Bartal, and X. Zhang, "An optical cloak made of dielectrics," *Nat. Mater.* **8**, 568–571 (2009).
6. R. Liu, X. M. Yang, J. G. Gollub, J. J. Mock, T. J. Cui, and D. R. Smith, "Gradient index circuit by waveguided metamaterials," *Appl. Phys. Lett.* **94**, 073506 (2009).
7. K. Preston, N. Sherwood-Droz, J. S. Levi, H. L. R. Lira, and M. Lipson, "Design rules for WDM optical interconnects using silicon microring resonators," (2011), submitted to *Opt. Express*.
8. R. K. Luneburg, *Mathematical Theory of Optics* (University of California Press, 1964).
9. U. Leonhardt and T. Philbin, *Geometry and Light: The Science of Invisibility* (Dover Publications, 2010).
10. T. Shoji, T. Tsuchizawa, T. Watanabe, K. Yamada, and H. Morita, "Low loss mode size converter from 0.3  $\mu\text{m}$  square Si wire waveguides to singlemode fibres," *Electron. Lett.* **38**, 1669 (2002).
11. V. R. Almeida, R. R. Panepucci, and M. Lipson, "Nanotaper for compact mode conversion," *Opt. Lett.* **28**, 1302 (2003).
12. K. K. Lee, D. R. Lim, D. Pan, C. Hoepfner, W.-Y. Oh, K. Wada, L. C. Kimerling, K. P. Yap, and M. T. Doan, "Mode transformer for miniaturized optical circuits," *Opt. Lett.* **30**, 498 (2005).
13. G. Roelkens, P. Dumon, W. Bogaerts, D. Van Thourhout, and R. Baets, "Efficient silicon-on-insulator fiber coupler fabricated using 248-nm-deep UV lithography," *IEEE Photon. Technol. Lett.* **17**, 2613–2615 (2005).
14. A. Di Falco, S. C. Kehr, and U. Leonhardt, "Luneburg lens in silicon photonics," *Opt. Express* **19**, 5156 (2011).
15. F. Zernike, "Luneburg lens for optical waveguide use," *Opt. Commun.* **12**, 379–381 (1974).
16. N. Kundtz and D. R. Smith, "Extreme-angle broadband metamaterial lens," *Nat. Mater.* **9**, 129–32 (2010).
17. H. F. Ma and T. J. Cui, "Three-dimensional broadband and broad-angle transformation-optics lens," *Nat. Commun.* **1**, 124 (2010).

18. T. Zentgraf, Y. Liu, M. H. Mikkelsen, J. Valentine, and X. Zhang, "Plasmonic Luneburg and Eaton lenses," *Nature Nanotechnol.* **6**, 151–155 (2011).
  19. J. Cardenas, C. B. Poitras, J. T. Robinson, K. Preston, L. Chen, and M. Lipson, "Low loss etchless silicon photonic waveguides," *Opt. Express* **17**, 4752 (2009).
- 

## 1. Introduction

Gradient index (GRIN) structures have received increased attention in recent literature, from invisibility cloaks and illusion devices, to planar lenses, such as Maxwell's fish eye. Fabrication of such structures, where the dielectric medium is modified rapidly on a few-wavelength scale, is challenging and limited by scattering losses introduced by discrete elements often used in the effective media [1–6]. We show here a low loss GRIN structure based on ultra-strong index variation with unique index variation profiles over  $30\ \mu\text{m}$  that drastically improves the tolerance of conventional fiber-to-waveguide links—a critical aspect for enabling future optical networks on chip [7]. The ability to fabricate GRIN structures with ultra-strong gradient can enable a whole new class of photonic devices with new functionalities for light propagation, optical signal processing, and imaging techniques in general.

Among GRIN structures, the Luneburg lens is of special interest and can be demonstrated using only dielectric materials. The Luneburg lens is an aberration-free and coma-free spherical lens whose focal points lie on a circumference around itself [8,9]. Rays incident from far away (i.e. with  $k$  vector parallel to the direction of propagation) at different positions will all focus on the same point on the circumference (Fig. 1b). This is in strong contrast to a conventional lens, where, due to aberrations, the focal point varies with the position of the incident light (Fig. 1a). In addition, unlike a conventional lens, the Luneburg is composed of a rotationally symmetric gradient refractive index  $n^2 = n_0^2(2 - \rho^2)$ , where  $n_0$  is constant and  $\rho$  is the normalized coordinate in the radial direction of the lens, shown in Fig. 1c. This way, one can choose the constant  $n_0$  to match the environment refractive index, and eliminate reflections at the lens interface.

The lack of sensitivity of the Luneburg lens to the exact position of the incoming light has strong applications for the robust coupling between photonic structures with very different scales. The integration of future optical communications from the fiber optical cable down to the microprocessor core will require efficient and reliable coupling devices, both at the fiber-to-chip and inter-chip levels. Low-loss, fiber-to-chip coupling can be achieved today via inverse tapers [10–13], which adiabatically convert the large modes coming from optical fibers into the tightly confined modes of integrated silicon waveguides. Nonetheless, to perform properly, these tapers have stringent alignment requirements, due to their high sensitivity [11]. The need thus arises for passive optical couplers that are robust to misalignment—a class of devices designed to reliably collect the energy delivered to the chip and couple it to the system's waveguides.

## 2. Design and fabrication

For applications in silicon photonics, the Luneburg lens is required to have a strong index variation over a short distance without introducing excessive loss. A Luneburg lens was recently demonstrated in silicon using a tapered waveguide for tailoring the index of refraction [14] by 41% over a disk of  $98\ \mu\text{m}$  radius. Here, in order to demonstrate a Luneburg lens for silicon photonics we tailor the index by 41% over  $15\ \mu\text{m}$ .

The gradient refractive index necessary for the Luneburg lens was implemented by controlling the thickness of the guiding layer of the device [14]. Light confinement in the direction normal to the device is achieved by total internal reflection between a guiding silicon layer and the top and bottom  $\text{SiO}_2$  claddings. The effective refractive index of this slab structure is dependent on the thickness of the silicon layer, such that the gradient refractive index required

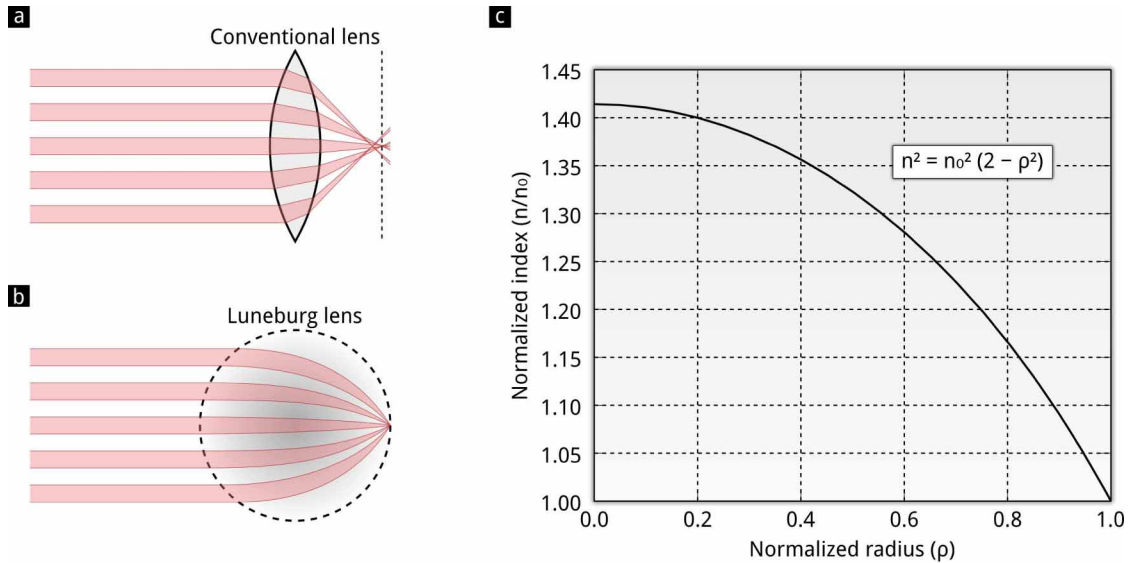


Fig. 1. (Color online) Comparison between a Luneburg and a standard lens. (a) The conventional lens creates a Fourier transform of the input image at its focal plane, distorted by aberrations. (b) The Luneburg lens does the same over a focal circumference without aberrations. (c) Instead of a constant refractive index, the Luneburg lens shows a refractive index that decreases radially.

by the Luneburg lens can be translated into a height map for the slab. We used the constant  $n_0$  to match the refractive index of the cladding and minimize reflections. As a consequence, the thickness of the silicon layer in our lens varies from 0 at the edges to 82 nm at its center. Other implementations of the Luneburg lens have been demonstrated in geometrical optics [15], microwaves [16, 17], and plasmonics [18].

In order to achieve the ultra-strong index variation in a small device with controlled scattering loss, we used a focused ion beam (FIB) to pattern the gray-scale Luneburg height profile, shown in fig. 2. The device was fabricated on a Silicon-On-Insulator (SOI) wafer with 250 nm device layer and 3  $\mu\text{m}$  buried  $\text{SiO}_2$ . The waveguide and taper were patterned in poly(methyl methacrylate) via e-beam lithography, then transferred to the silicon layer via inductively coupled plasma, reactive ion etching (ICP-RIE). After that, the Luneburg lens was patterned using a calibrated FIB, and covered in approximately 2  $\mu\text{m}$  of  $\text{SiO}_2$  via plasma-enhanced, chemical vapor deposition (PECVD). The alignment precision we can obtain in our FIB tool is on the order of 1  $\mu\text{m}$ .

We measured the gradient height profile patterned via FIB with an atomic force microscope (AFM), displayed in Fig. 2a. The fabricated profile is compared to the theoretical one in Fig 2b, where we can see a very good match. Analysis of the data revealed that the surface of the lens has roughness around 2 nm on the bulk, and a larger variation around the edges, mainly due to the variation in height of the regions outside the perimeter of the lens (completely etched towards the lower-left and with full height towards the upper-right in Fig. 2a).

### 3. Experimental results

We measured the sensitivity of the Luneburg-mediated coupler against misalignment and compared it to a reference silicon waveguide terminated with an inverse taper [11]. The inverse taper

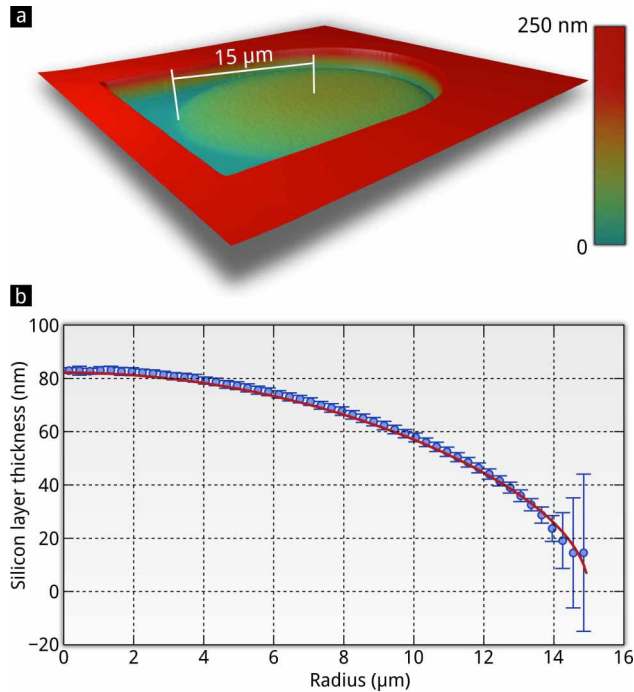


Fig. 2. (Color online) Characterization of the FIB patterning process. (a) AFM scan from a Luneburg lens patterned via FIB with thickness varying from 0 to 82 nm. (b) Comparison between the fabricated (circles) and the required (continuous line) lens profiles. The measured RMS surface roughness is around 2 nm for most of the surface, with exception of approximately 1  $\mu\text{m}$  around the edge, where imperfections are due to the abrupt change in the silicon depth.

is used here in order to account for the spot size at the focal point limited by the  $k$ -distribution of the incoming fiber. We show that for a fiber-to-waveguide coupler mediated by a Luneburg lens, even if the fiber is offset from the optical axis of the inverse taper, the lens will focus light at the taper tip, minimizing the alignment sensitivity of the coupling. Figure 3 illustrates this process and shows a microscope image of the device fabricated on silicon. The taper was 75- $\mu\text{m}$  long, with width increasing linearly from 120 nm at its tip to 450 nm at the silicon waveguide. Light at 1.55- $\mu\text{m}$  wavelength was coupled via a lensed optical fiber mounted on a piezoelectric stage. The fiber produced a focused beam at the edge of the sample with approximately 3  $\mu\text{m}$  in diameter (see a schematic in Figs. 3a and 3b). The size of the spot produced at the focal point of the Luneburg lens depends on the input beam profile in the same way as in a conventional lens. Thus, by using a lensed fiber with focus on the chip edge, we minimize the spot size at the focal point of the Luneburg lens, whereas additional  $k$ -vector contributions in the input beam would increase the spot size at the focal point. The output signal was collected via a 10 $\times$  objective, filtered to keep only the TE mode (for which the Luneburg lens was designed), and sent to a photo-detector.

We demonstrate robust fiber-to-waveguide coupling with decreased misalignment sensitivity: over 6 dB power gain over a reference taper at 4- $\mu\text{m}$  misalignment. The misalignment loss, measured by scanning the piezoelectric stage across the coupling region, is plotted in Fig. 4 for 4 different devices: 2 Luneburg-mediated couplers (blue circles and squares), and 2 reference tapers (red circles and squares). One can clearly see that, as expected, the Luneburg lens

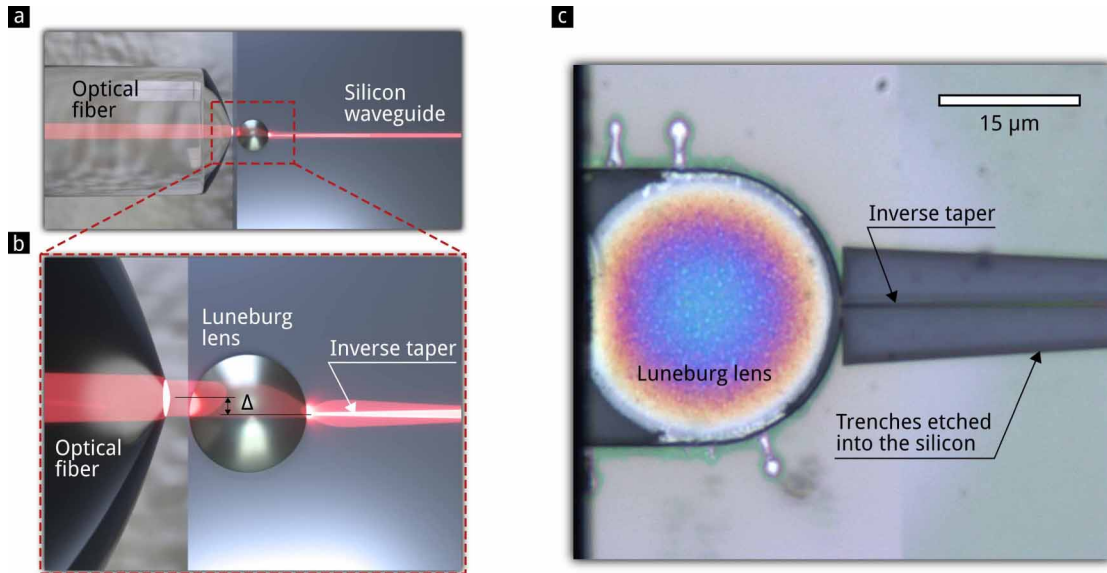


Fig. 3. (Color online) Fiber-to-chip coupler based on the Luneburg lens. (a) A lensed fiber is used to couple light into the silicon waveguide. (b) Zoomed-in illustration of the coupling region. We add a Luneburg lens to the conventional inverse taper design to minimize losses induced by the misalignment  $\Delta$ . (c) Optical microscope image of the fabricated device. The trenches defining the waveguide and taper are due to the use of positive resist. The variation of the silicon layer thickness in the lens can be clearly seen by the interference pattern (colors) in the image. Note that the dark area on the left edge of the image is due to face polishing, i.e., the lens has not been damaged.

decreases the losses introduced by misalignment. Note, however, that these measurements are normalized by the power detected with no misalignment for each device, at which position the total insertion loss of the Luneburg-mediated couplers was approximately 6.5 dB higher than the reference. We believe that the fabrication process is responsible for this additional insertion loss. The FIB patterning introduces partial amorphization of the silicon layer, as well as gallium implantation, and a small roughness on the surface of the lens, which in principle could be decreased using annealing and controlled oxidation [19]. Additionally, misalignment between the lens and the inverse taper may also increase the insertion loss, but this could be mitigated with improved alignment control in the patterning tool.

The continuous lines in Fig. 4 are results from full 3-d simulations performed with COMSOL Multiphysics<sup>®</sup>. The simulation includes a lens with the same diameter as the tested device, plus the taper region, and a Gaussian source with standard deviation  $\sigma = 3\ \mu\text{m}$  placed  $1\ \mu\text{m}$  from the device input facet (in air). The simulated results showed that the inclusion of the Luneburg lens has no fundamental impact in the total insertion loss of our structure, confirming our expectations that the additional losses are due to imperfections in the fabrication, and they show a good match for the alignment sensitivity.

#### 4. Conclusion

Silicon-based compact GRIN structures, including the demonstrated here Luneburg-mediated coupler, pave the way to a class of ultra-compact GRIN devices with novel photonic properties including aberration-free imaging, advanced optical signal processing, and mode multiplexing

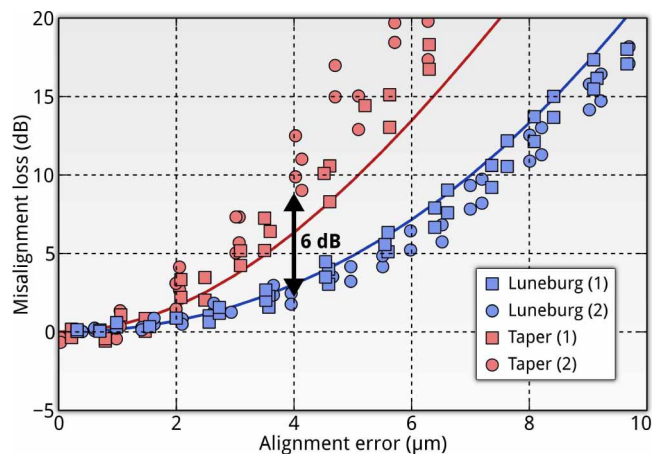


Fig. 4. (Color online) Experimental results for the alignment sensitivity of the coupler devices. Two Luneburg-based devices (blue) and 2 bare taper couplers (red) are measured. One can clearly see that the introduction of the Luneburg lens improves the robustness to misalignment. Full 3-d simulations (continuous lines) match the experimental results very well.

for applications in integrated optics and silicon photonics such as optical coherent imaging, and telecommunication networks.

#### Acknowledgments

The authors would like to acknowledge the support of Cornell's Center for Nanoscale Systems (CNS), funded by the National Science Foundation. This work was performed in part at the Cornell Nanoscale Facility, a member of the National Nanotechnology Infrastructure Network, which is supported by the National Science Foundation. This work has been supported by the AFOSR MURI for Complex and Robust On-chip Nanophotonics (Dr. Gernot Pomrenke), grant number FA9550-09-1-0704.